



From the Cover

- 4404 Mangrove trees and carbon sequestration
- E2218 Phase transition in semidefinite programming
- E2326 Endogenous retroviruses in human populations
- 4266 Black carbon and urban environments
- 4398 Nitrogen fixation in the South Pacific

Contents

THIS WEEK IN PNAS

- 4231 In This Issue

LETTERS (ONLINE ONLY)

- E2209 Anthropogenic aerosols are a potential cause for migration of the summer monsoon rain belt in China
Shaocai Yu, Pengfei Li, Liqiang Wang, Peng Wang, Si Wang, Shucheng Chang, Weiping Liu, and Kiran Alapaty
- E2211 Reply to Yu et al.: Global temperature change as the ultimate driver of the shift in the summer monsoon rain belt in East Asia
Shiling Yang, Zhongli Ding, Yangyang Li, Xu Wang, Wenying Jiang, and Xiaofang Huang
- E2213 Reply to Stoet and Geary: Effects of gendered behavior on testosterone, not sex differences, as research focus
Sari M. van Anders, Katherine L. Goldey, and Jeffrey Steiger
- E2215 Emergence of sociocultural norms restricting intermarriage in large social strata (endogamy) coincides with foreign invasions of India
Murali K. Vadivelu

SCIENCE AND CULTURE—How science intersects with culture

- 4234 Terraforming a volcano, artfully
Amber Dance

INNER WORKINGS—An over-the-shoulder look at scientists at work

- 4236 A big role for a microbial parasite
Karen Hopkin

COMMENTARIES

- 4238 Inference on graphs via semidefinite programming
Afonso S. Bandeira
→ See companion article on page E2218
- 4240 HERV-K HML-2 diversity among humans
Jack Lenz
→ See companion article on page E2326

Cover image: Pictured are red mangrove trees in La Encrucijada Biosphere Reserve, Mexico. Paula Ezcurra et al. studied short, stubby mangroves growing on layers of root peat that accumulated over thousands of years along the desert coasts of Baja California, and found that the desert mangroves harbor more belowground carbon than some of the tallest tropical mangroves of the Mexican Pacific coast. The findings suggest that the dryland mangroves represent a large carbon sink in Mexico's northern deserts and highlight the importance of mangrove conservation in the region. See the article by Ezcurra et al. on pages 4404–4409. Image courtesy of Octavio Aburto-Oropeza.

BIOCHEMISTRY

- E2258 Cellular uptake and anticancer activity of carboxylated gallium corroles**
Melanie Pribisko, Joshua Palmer, Robert H. Grubbs, Harry B. Gray, John Termini, and Punrajit Lim
- E2267 Functional architecture of the Reb1-Ter complex of *Schizosaccharomyces pombe***
Rahul Jaiswal, Malay Choudhury, Shamsu Zaman, Samarendra Singh, Vishaka Santosh, Deepak Bastia, and Carlos R. Escalante
- E2277 Kinetic selection vs. free energy of DNA base pairing in control of polymerase fidelity**
Kerian Oertell, Emily M. Harcourt, Michael G. Mohsen, John Petruska, Eric T. Kool, and Myron F. Goodman
- 4252 Individual variability in human blood metabolites identifies age-related differences**
 Romanas Chaleckis, Itsuo Murakami, Junko Takada, Hiroshi Kondoh, and Mitsuhiro Yanagida
- 4302 Mass-tag labeling reveals site-specific and endogenous levels of protein S-fatty acylation**
Avital Percher, Srinivasan Ramakrishnan, Emmanuelle Thinson, Xiaoqiu Yuan, Jacob S. Yount, and Howard C. Hang
- 4308 Mechanism for accurate, protein-assisted DNA annealing by *Deinococcus radiodurans* DdrB**
Seiji N. Sugiman-Marangos, Yoni M. Weiss, and Murray S. Junop
- 4314 Lenz-Majewski mutations in *PTDSS1* affect phosphatidylinositol 4-phosphate metabolism at ER-PM and ER-Golgi junctions**
Mira Sohn, Pavlina Ivanova, H. Alex Brown, Daniel J. Toth, Peter Varnai, Yeun Ju Kim, and Tamas Balla
- 4320 Metabolomics-assisted proteomics identifies succinylation and SIRT5 as important regulators of cardiac function**
Sushabhan Sadhukhan, Xiaojing Liu, Dongryeol Ryu, Ornella D. Nelson, John A. Stupinski, Zhi Li, Wei Chen, Sheng Zhang, Robert S. Weiss, Jason W. Locasale, Johan Auwerx, and Hening Lin
- 4326 Asymmetric arginine dimethylation of RelA provides a repressive mark to modulate TNF α /NF- κ B response**
 Anja Reintjes, Julian E. Fuchs, Leopold Kremser, Herbert H. Lindner, Klaus R. Liedl, Lukas A. Huber, and Taras Valovka

BIOPHYSICS AND COMPUTATIONAL BIOLOGY

- E2286 Inhibition of translation initiation complex formation by GE81112 unravels a 16S rRNA structural switch involved in P-site decoding**
Attilio Fabbretti, Andreas Schedlbauer, Letizia Brandi, Tatsuya Kaminishi, Anna Maria Giuliadori, Raffaella Garofalo, Borja Ochoa-Lizarralde, Chie Takemoto, Shigeyuki Yokoyama, Sean R. Connell, Claudio O. Gualerzi, and Paola Fucini
- E2296 Twist-open mechanism of DNA damage recognition by the Rad4/XPC nucleotide excision repair complex**
 Yogambigai Velmurugu, Xuejing Chen, Phillip Slogoff Sevilla, Jung-Hyun Min, and Anjum Ansari
- 4332 Surface force measurements and simulations of mussel-derived peptide adhesives on wet organic surfaces**
Zachary A. Levine, Michael V. Rapp, Wei Wei, Ryan Gotchy Mullen, Chun Wu, Gül H. Zerze, Jeetain Mittal, J. Herbert Waite, Jacob N. Israelachvili, and Joan-Emma Shea
- 4338 Simultaneous single-molecule epigenetic imaging of DNA methylation and hydroxymethylation**
Chun-Xiao Song, Jiajie Diao, Axel T. Brunger, and Stephen R. Quake

- 4344 Pathogen receptor discovery with a microfluidic human membrane protein array**
Yair Glick, Ya'ara Ben-Ari, Nir Drayman, Michal Pellach, Gregory Neveu, Jim Boonyaratankornkit, Dorit Avrahami, Shirir Einav, Ariella Oppenheim, and Doron Gerber

CELL BIOLOGY

- E2306 PDGF-AB and 5-Azacytidine induce conversion of somatic cells into tissue-regenerative multipotent stem cells**
Vashe Chandrakanthan, Avani Yeola, Jair C. Kwan, Rema A. Oliver, Qiao Qiao, Young Chan Kang, Peter Zazour, Dominik Beck, Lies Boelen, Ashwin Unnikrishnan, Jeanette E. Villanueva, Andrea C. Nunez, Kathy Knezevic, Cintia Palu, Rabab Nasrallah, Michael Carnell, Alex Macmillan, Renee Whan, Yan Yu, Philip Hardy, Shane T. Grey, Amadeus Gladbach, Fabien Delerue, Lars Ittner, Ralph Mobbs, Carl R. Walkley, Louise E. Purton, Robyn L. Ward, Jason W. H. Wong, Luke B. Hesson, William Walsh, and John E. Pimanda
- 4350 Neutrophil-derived alpha defensins control inflammation by inhibiting macrophage mRNA translation**
Matthew Brook, Gareth H. Tomlinson, Katherine Miles, Richard W. P. Smith, Adriano G. Rossi, Pieter S. Hiemstra, Emily F. A. van 't Wout, Jonathan L. E. Dean, Nicola K. Gray, Wuyuan Lu, and Mohini Gray
- 4356 Heterotrimeric G-protein shuttling via Gip1 extends the dynamic range of eukaryotic chemotaxis**
Yoichiro Kamimura, Yukihiko Miyana, and Masahiro Ueda
- 4362 Extended synaptotagmins are Ca²⁺-dependent lipid transfer proteins at membrane contact sites**
Haijia Yu, Yinghui Liu, Daniel R. Gulbranson, Alex Paine, Shailendra S. Rathore, and Jingshi Shen
- 4368 Axial superresolution via multiangle TIRF microscopy with sequential imaging and photobleaching**
Yan Fu, Peter W. Winter, Raul Rojas, Victor Wang, Matthew McAuliffe, and George H. Patterson

ECOLOGY

- 4374 Slow climate velocities of mountain streams portend their role as refugia for cold-water biodiversity**
Daniel J. Isaak, Michael K. Young, Charles H. Luce, Steven W. Hostetler, Seth J. Wenger, Erin E. Peterson, Jay M. Ver Hoef, Matthew C. Groce, Dona L. Horan, and David E. Nagel
- 4380 Species interactions slow warming-induced upward shifts of treelines on the Tibetan Plateau**
Eryuan Liang, Yafeng Wang, Shilong Piao, Xiaoming Lu, Jesús Julio Camarero, Haifeng Zhu, Liping Zhu, Aaron M. Ellison, Philippe Ciais, and Josep Peñuelas
- 4386 Test of the invasive pathogen hypothesis of bumble bee decline in North America**
Sydney A. Cameron, Haw Chuan Lim, Jeffrey D. Lozier, Michelle A. Duennes, and Robbin Thorp

ENVIRONMENTAL SCIENCES

- 4392 Photodegradation alleviates the lignin bottleneck for carbon turnover in terrestrial ecosystems**
Amy T. Austin, M. Soledad Méndez, and Carlos L. Ballaré
- 4398 Low rates of nitrogen fixation in eastern tropical South Pacific surface waters**
Angela N. Knapp, Karen L. Casciotti, William M. Berelson, Maria G. Prokopenko, and Douglas G. Capone
→ See Commentary on page 4246
- 4404 Coastal landforms and accumulation of mangrove peat increase carbon sequestration and storage**
 Paula Ezcurra, Exequiel Ezcurra, Pedro P. Garcillán, Matthew T. Costa, and Octavio Aburto-Oropeza

Coastal landforms and accumulation of mangrove peat increase carbon sequestration and storage

Paula Ezcurra^{a,1}, Exequiel Ezcurra^b, Pedro P. Garcillán^c, Matthew T. Costa^a, and Octavio Aburto-Oropeza^a

^aMarine Biology Research Division, Scripps Institution of Oceanography, La Jolla, CA 92093; ^bDepartment of Botany and Plant Sciences, University of California, Riverside, CA 92521; and ^cCentro de Investigaciones Biológicas del Noroeste, Playa Palo de Santa Rita Sur, La Paz, Baja California Sur 23096, Mexico

Edited by Rodolfo Dirzo, Stanford University, Stanford, CA, and approved February 23, 2016 (received for review October 8, 2015)

Given their relatively small area, mangroves and their organic sediments are of disproportionate importance to global carbon sequestration and carbon storage. Peat deposition and preservation allows some mangroves to accrete vertically and keep pace with sea-level rise by growing on their own root remains. In this study we show that mangroves in desert inlets in the coasts of the Baja California have been accumulating root peat for nearly 2,000 y and harbor a belowground carbon content of 900–34,00 Mg C/ha, with an average value of 1,130 (\pm 128) Mg C/ha, and a belowground carbon accumulation similar to that found under some of the tallest tropical mangroves in the Mexican Pacific coast. The depth–age curve for the mangrove sediments of Baja California indicates that sea level in the peninsula has been rising at a mean rate of 0.70 mm/y (\pm 0.07) during the last 17 centuries, a value similar to the rates of sea-level rise estimated for the Caribbean during a comparable period. By accreting on their own accumulated peat, these desert mangroves store large amounts of carbon in their sediments. We estimate that mangroves and halophyte scrubs in Mexico's arid northwest, with less than 1% of the terrestrial area, store in their belowground sediments around 28% of the total belowground carbon pool of the whole region.

blue carbon | carbon sequestration | mangroves | peat | Baja California

Many studies have highlighted the importance of mangroves and other coastal ecosystems in belowground carbon storage. Duarte and Cebrían (1) showed that mangroves allocate ca. 40% of their net primary productivity (NPP) to excess photosynthetic carbon that is either exported to lagoon and ocean waters or stored underground. According to these authors, marine angiosperms, which contribute only 4% of total ocean NPP, generate ca. 30% of total ocean carbon storage. Based on data from the Indo-Pacific region, Donato et al. (2) (also see Murdiyarto et al., ref. 3) concluded that mangroves are among the most carbon-rich tropical forests in the world, containing on average 1,023 Mg C/ha, and estimated that the organic-rich soils of mangrove swamps account for the majority (71–98%) of total carbon storage in estuarine ecosystems. Similarly, in a review paper on the role of vegetated coastal habitats in sequestering atmospheric CO₂, Mcleod et al. (4) concluded that, globally, mangroves have a disproportionate importance in sequestering and storing carbon within their sediments. Other studies (5, 6) have highlighted the large economic value of mangroves as carbon sinks and their potential role in reducing carbon emissions from forest loss. None of these papers, however, analyzes the natural history of the belowground carbon stored in mangrove sediments.

Exploring the long-term vertical accretion of mangroves in relation to Holocene sea-level rise, other authors have devoted considerable effort to describing the nature of belowground organic matter in mangrove forests. For example, Toscano and Macintyre (7) were able to construct a Holocene sea-level curve for the western Atlantic using ¹⁴C radioisotopic dating of coral reef cores and mangrove peat from the Florida Keys and Belize. Following on this work, researchers in Florida and the Caribbean have shown that peat formation has allowed Caribbean mangroves

to rise gradually on their own peat during the Holocene, thus adjusting to rising sea levels (8, 9). These studies have shown that biotic processes, namely the subsurface accumulation of refractory mangrove roots, or mangrove “peat” (10, 11), have allowed mangroves in Caribbean cays to adjust to the rising sea levels that took place globally during the Holocene after the last Pleistocene glaciation. None of these studies on peat formation, vertical accretion, and Holocene sea-level rise has framed its results in terms of rates of carbon sequestration or belowground carbon storage, with the exception of Adame et al. (12), who used a volcanic ash sedimentary layer as a dating point to estimate the rate of carbon sequestration in La Encrucijada Lagoon in Chiapas, Mexico.

There clearly are differences in the approach taken by each school of research in the study of belowground organic matter in mangrove sediments. Researchers studying vertical accretion and sea-level rise emphasize the role of mangrove peat (i.e., partially decomposed, fibrous remains of mangrove tissues) and discuss under what conditions peat, as opposed to amorphous organic matter or “muck,” forms (9–11). In contrast, studies on belowground sequestration do not make a clear distinction between peaty and amorphous remains of belowground mangrove tissues. Donato et al. (2) for example, described mangrove soils as consisting of a “tidally submerged suboxic layer (variously called ‘peat’ or ‘muck’) supporting anaerobic decomposition pathways and having moderate to high C concentration.”

However, the difference between peat and muck in the study of carbon sequestration in wetlands is important. Mangrove muck, as found, for example, in *Avicennia* mudflats, is a mixture of mineral sediments and finely disintegrated organic matter that has been thoroughly mixed by bioturbation from burrowing crabs

Significance

Despite their small height and stunted appearance, mangroves along the desert coasts of Baja California have compensated for sea-level rise during the last two millennia by accreting on their own root remains. In doing so, they have accumulated very large amounts of carbon in their sediments (900–3,000 Mg C/ha), often higher than that accumulated under tall, lush, tropical mangrove forests. Mangroves represent the largest carbon sink per unit area in Mexico's northern drylands. Our results highlight the global importance of mangrove conservation in this region.

Author contributions: P.E., E.E., M.T.C., and O.A.-O. designed research; P.E., E.E., P.P.G., and M.T.C. performed research; P.E., E.E., and M.T.C. analyzed data; and P.E., E.E., P.P.G., M.T.C., and O.A.-O. wrote the paper.

The authors declare no conflict of interest.

This article is a PNAS Direct Submission.

Freely available online through the PNAS open access option.

Data deposition: The sampling data reported in this paper have been deposited in Dryad (dx.doi.org/10.5061/dryad.5k0g4).

¹To whom correspondence should be addressed. Email: pezcurra@ucsd.edu.

This article contains supporting information online at www.pnas.org/lookup/suppl/doi:10.1073/pnas.1519774113/-DCSupplemental.

and other invertebrates as well as by abiotic processes (13). Because muck lacks identifiable organic fragments and is commonly highly mixed, core samples cannot be used reliably for radiocarbon dating. Peat, in contrast, is a brown-reddish, fibrous network of only partially decomposed rootlets that are susceptible to botanical identification. Peat presents an invaluable record of changes in the environment through recognizable fragments of plant tissue (14) that can be used to identify the origin of stored carbon and to date the age of the fragments through radiocarbon methods. Despite its potential importance in estimating carbon sequestration rates, little is known about the conditions under which mangrove peat forms and the role it plays in belowground carbon storage in tropical coastal wetlands.

The disproportionate contribution of mangrove ecosystems to global carbon sequestration is particularly noticeable in desert environments. Using a research aircraft to estimate land-atmosphere CO_2 fluxes, Zulueta et al. (15) found that in the desert coast of Bahía Magdalena in Baja California Sur, Mexico, midday uptake was $1.32 \mu\text{mol CO}_2\text{-m}^{-2}\text{-s}^{-1}$ above the desert and was six to seven times higher ($8.11 \mu\text{mol CO}_2\text{-m}^{-2}\text{-s}^{-1}$) in the lagoon mangroves. Only a small fraction (ca. $0.7 \mu\text{mol CO}_2\text{-m}^{-2}\text{-s}^{-1}$) of this high productivity is exported (16).

Two broad questions arise from these results. The first is how much of the carbon uptake performed by desert mangroves is stored in their sediment, and how this storage compares with that in other, more tropical mangroves and desert ecosystems. The second question is in what form, peat or muck, belowground carbon accumulates in desert mangroves. As discussed previously, the question is important because peat lends itself to radiocarbon dating and allows the estimation of historic carbon sequestration rates. In regard to this second question we wanted to achieve three specific goals: (i) to identify the conditions under which peat forms in the sedimentary profile; (ii) to identify the species responsible for peat formation; and (iii) to evaluate the importance of peat formation for belowground carbon storage.

We tested these questions in four locations. Two were in Baja California, representing extreme landscape variations within the desert mangroves of northern Mexico. The first location, Bahía Magdalena, is on a very flat coastal plain on the Pacific side of the peninsula; the second, Balandra, sits on the Gulf of California side and is enclosed by mountains (Fig. S1 B and C). We then compared these locations with the two largest tropical mangroves along the Pacific Coast of Mexico: Marismas Nacionales, in the state of Nayarit, and La Encrucijada, in Chiapas near the Guatemalan border (Fig. S1A).

Results

Total Belowground Carbon.

Bahía Magdalena. Overall, Bahía Magdalena, a non-topographically constrained desert lagoon on a flat coastal plain, had the second lowest belowground carbon values of all sampled locations (Fig. 1A). The sediments in the upper mudflats and hinterlands were low in carbon content ($<200 \text{ Mg C/ha}$; sample depth 0.9–1.6 m), but, in contrast, the *Rhizophora* fringe forests had total carbon contents of ca. 500 Mg C/ha (sample depth 1.3–1.5 m). Additionally, a receding mangrove fringe coast, where old peat was visibly being washed away by the waves, had a total carbon content of 440 Mg C/ha (sample depth 1.3 m), suggesting that this ecosystem did sequester and accumulate large amounts of carbon in the past.

Balandra. A topographically constrained lagoon, Balandra had the highest belowground carbon values for *Avicennia germinans* of all locations sampled, both mudflat and hinterland, ranging between 400 – $1,300 \text{ Mg C/ha}$ (sample depth 0.6–2.3 m). Much of this carbon is found in the form of fibrous root fragments or mangrove peat. One *Rhizophora* fringe forest had 894 Mg C/ha (sample depth 0.6 m), and a second one had only 279 Mg C/ha (sample depth 2.0 m), possibly because this forest is expanding into the lagoon and growing on a relatively shallow bank of calcite (Fig. 1B).

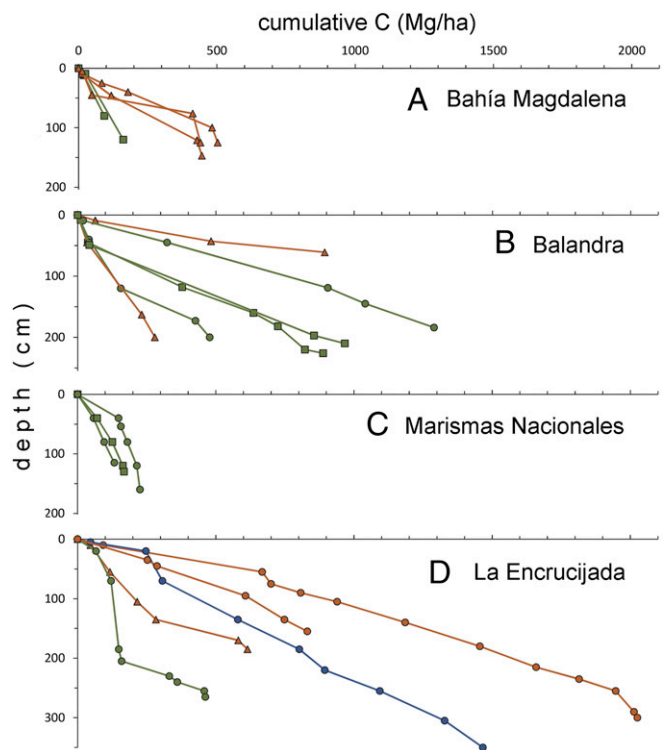


Fig. 1. Cumulative belowground carbon content in the sample cores. (A) Bahía Magdalena. (B) Balandra. (C) Marismas Nacionales. (D) La Encrucijada. Sites are arranged in descending latitudinal order. The symbols describe the landform where the core was taken: forest fringe (■), mudflat (●), and upper mudflat/hinterland (▼). The color of the series describes the dominant species: *R. mangle* (red), *A. germinans* (green), and *P. aquatica* (blue).

Marismas Nacionales. Despite the large extent of these coastal swamplands, the dominant *Avicennia* forest of Marismas Nacionales had the lowest belowground carbon values of all four sites, with all cores indicating less than 300 Mg C/ha (sample depth 1.2–1.6 m) (Fig. 1C). Furthermore, all the carbon in the mangrove sediments in Marismas Nacionales was present in the form of muck, and no visible fragments of fibrous peat were found in the sedimentary profiles of the three sites.

La Encrucijada. A tropical mangrove in a high-precipitation area, La Encrucijada had the deepest and most carbon-rich sediments of the four locations, with one 3-m-deep *Rhizophora* mudflat core reaching over $2,000 \text{ Mg C/ha}$. The lowest carbon values, in a *Rhizophora* fringe and an *Avicennia* mudflat, were both still high compared with Marismas Nacionales and Bahía Magdalena (Fig. 1D). The only nonmangrove core, a *Pachira aquatica* forest growing in a waterlogged freshwater mudflat, had ca. $1,500 \text{ Mg C/ha}$ (sample depth 3.5 m) and was the deepest core overall.

Origin of Mangrove Peat. There was a general correlation between the amount of carbon stored at each location and the nature of the organic matter in the sediment profile. Marismas Nacionales, the location with the lowest amount of belowground carbon, had only muck in the mangrove sediment profile. In contrast, the locations with the highest amounts of carbon in their sediments, Balandra and La Encrucijada, had large layers of fibrous, partially decomposed root remains in the sediment profile (Dataset S1). Observations of these peaty sediments under a dissection microscope showed that in old samples, deep in the sediment layers, the root cortex remains undecomposed and is still clearly identifiable. Microscopic staining of root cortical tissues from living individuals showed a consistent distinction between species. Roots of *A. germinans* have rows of longitudinally

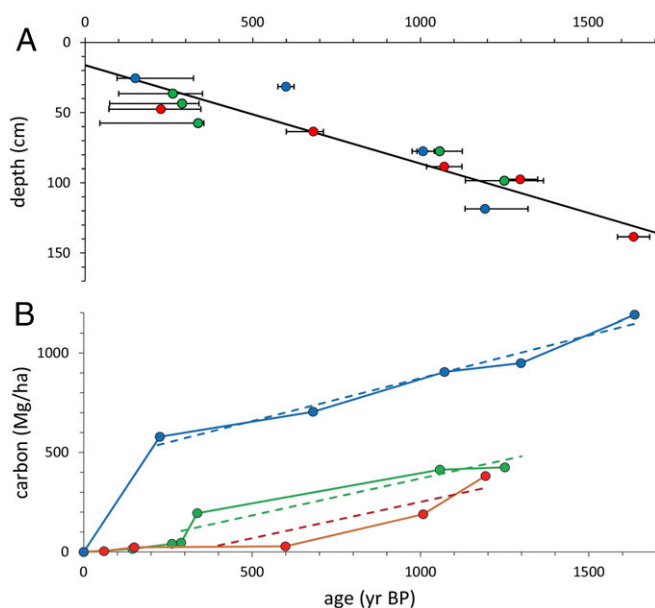


Fig. 2. Peat age and carbon content. (A) ^{14}C dating of peat fragments collected in the sediment profile plotted against depth (below mean sea level) for three mangrove cores: a dead, receding fringe in Bahia Magdalena (green), a halophyte hinterland with dwarfed *Avicennia* in Balandra (red), and a mudflat with dense stands of *Avicennia* in Balandra (blue). Regardless of the current status of the site, the age–depth relationship is consistent across peat cores ($r^2 = 0.87$, $P < 0.0001$). The regression line shows the inferred rate of sea-level rise for the last 1,600 y (0.70 ± 0.07 mm/y). (B) Cumulative belowground carbon content in the same three mangrove cores in Baja California as a function of age of the sedimentary layer. In the *Avicennia* mudflat, carbon has been actively sequestered below ground during recent centuries. In the other two sites carbon sequestration was intense more than 300–600 y B.P. but now is low. The dashed lines represent the major axis fit showing that total carbon content in older peat layers scales up with age of the sediment at similar rates for all three sites.

elongated epidermal cells measuring *ca.* 50–70 μm long and 10–20 μm wide, whereas those of *Rhizophora mangle* are shorter and wider [described as “root cortex short cells” by Gill and Tomlinson (17)], measuring 20–30 μm long and 30–40 μm wide (Fig. S2). With this identification process we could recognize the origin of the peat layers at each location.

We found that at Balandra the large deposits of peat were derived from the growth and accumulation of *Avicennia* roots in the sediment under a 20- to 40-cm-deep surface layer of mud. At La Encrucijada, in contrast, peat is formed chiefly on the ground surface of the *Rhizophora* mudflat, around the tangle of stilt roots that reach the ground from the tree stems and branches.

Belowground Carbon Age. The age of the cored sediments in Baja California at their deepest sample ranged between 1,193 and 1,636 y B.P. In Bahía Magdalena we sampled a receding coastal fringe with no live vegetation (only dead mangrove stumps). Although currently there are no live roots, the sediment profile was rich in old, eroding peat whose age at 1 m depth dated back to 1,250 y B.P. (Fig. 2A). In the Balandra lagoon (north) we cored a dense *Avicennia* mudflat, whose deepest (and oldest) sample dated 1,193 y B.P. at a depth of 1.3 m, giving way below to a shell calcite layer that dated 5,990 y B.P. In the southern part of Balandra we cored a halophytic hinterland populated by low halophilic vegetation and some sparse, stunted *Avicennia*. Below the first meter we hit a layer of old *Avicennia* peat, whose deepest sample dated 1,636 y B.P. at a depth of 1.40 m below the flooded mudflat level. Plotting the calibrated ^{14}C age of each peat sample in the three cores against the depth of the sample

below the flooded mudflat level, we found a very significant linear trend ($r^2 = 0.87$, $P < 0.0001$) with a slope of 0.070 ± 0.007 cm/y (Fig. 2A).

Carbon Accumulation Rates. Belowground carbon sequestration rates during recent decades varied from very low (*ca.* 0.1 $\text{Mg C}\cdot\text{ha}^{-1}\cdot\text{y}^{-1}$) in a receding fringe in Bahía Magdalena or a halophilic hinterland in Balandra to 2.6–6.3 $\text{Mg C}\cdot\text{ha}^{-1}\cdot\text{y}^{-1}$ in a *Rhizophora* mudflat in La Encrucijada (Table 1). The sequestration rates in healthy, productive *Avicennia* mudflats were *ca.* 2.6 $\text{Mg C}\cdot\text{ha}^{-1}\cdot\text{y}^{-1}$ in both the desert and the tropics, and were 6.9 $\text{Mg C}\cdot\text{ha}^{-1}\cdot\text{y}^{-1}$ in the freshwater *P. aquatica* swamp forest.

Plotting the cumulative belowground carbon content against the age of the sedimentary layer in three sites in Baja California, we found that the three cores differed in their initial rates: The *Avicennia* mudflat at Balandra showed a relatively high carbon sequestration rate during the last two centuries (2.56 $\text{Mg C}\cdot\text{ha}^{-1}\cdot\text{y}^{-1}$), but beyond that point the slope of the carbon–age curve stabilized at 0.43 (SE ± 0.04) $\text{Mg C}\cdot\text{ha}^{-1}\cdot\text{y}^{-1}$ (Fig. 2B). In contrast, both the halophyte hinterland in Balandra and the receding dead fringe in Bahía Magdalena have sequestered almost no carbon during the last five and three centuries, respectively, but before those dates the slopes of the curves (0.365 ± 0.12 and 0.371 ± 0.08 $\text{Mg C}\cdot\text{ha}^{-1}\cdot\text{y}^{-1}$, respectively) were similar to that found in the *Avicennia* mudflat.

Belowground Carbon in Other Desert Mangroves. In the other four rocky inlets we sampled, the vertical accretion with deep peat deposits in the *Avicennia* mudflats was similar to that in Balandra. The amounts of belowground carbon under the mudflats in these inlets ranged from 903 to 3,431 $\text{Mg C}/\text{ha}$, with an average of 1,130 (± 128) $\text{Mg C}/\text{ha}$ (Fig. S3). These results confirmed that peat formation and vertical accretion tend to develop in topographically constrained mangroves. Furthermore, many of the halophyte hinterlands that are found upslope of the *Avicennia* mudflats also can contain important amounts of peat and muck derived from past occupation of these habitats by mudflat forests. Pooling all our samples from Baja California, we found that, on average, mangrove hinterlands contain some 232 (± 106) $\text{Mg C}/\text{ha}$.

Geographic Analysis. In Mexico, the Sonoran Desert covers 211,967 km^2 , and the Sinaloan and Cape Region tropical thornscrubs cover 23,973 km^2 . On average, warm deserts and tropical drylands store 14 and 20 $\text{Mg C}/\text{ha}$ of belowground organic carbon, respectively (18, 19), so these ecosystems jointly store some 345 Tg of belowground carbon. The mangroves in the coasts of these ecoregions cover 1,162 km^2 , of which ~ 835 km^2 correspond to sedimentary coastal plains and the rest to spatially restricted

Table 1. Short-term carbon sequestration rates

Site	Landform	Dating method	Rate (range)
Bahía Magdalena	Dead fringe	^{14}C	0.10 (0.19–0.04)
Balandra	Hinterland	^{14}C	0.16 (0.25–0.07)
Balandra	<i>Avicennia</i> mudflat	^{14}C	2.56 (8.15–1.68)
La Encrucijada	<i>Avicennia</i> mudflat	^{14}C	2.56 (2.56–2.55)
La Encrucijada	<i>Rhizophora</i> mudflat	Ash layer	2.57
La Encrucijada	<i>Rhizophora</i> mudflat	^{14}C	6.25 (5.77–8.32)
La Encrucijada	<i>Pachira</i> mudflat	^{14}C	6.96 (7.04–6.90)

Mean carbon sequestration rates and error range in recent decades for seven sampling locations (measured in megagrams of carbon per hectare per year). In the sites where the rate was estimated using ^{14}C dating, the rate was calculated from the carbon accumulated over the last century. For the site where the rate was estimated using the Santa María volcanic ash layer as a dating reference, the rate was calculated over 112.1 y (October 1902–December 2014) from the carbon accumulated above the ash layer.

mangroves in abrupt shores and rocky islands. The mudflat and fringe forests we studied in Baja California (excluding two recently colonized sites, a hinterland in Bahía Magdalena and a fringe in Balandra) yielded an average of 463 (± 20) Mg C/ha in Bahía Magdalena and 1,130 (± 128) Mg C/ha in Balandra. Multiplying these values by the total area of coastal plain and spatially restricted mangroves, we reached a value of 76 Tg of belowground carbon storage for the regional mangroves. If we add to this value the amount of carbon below halophyte hinterlands (200 Mg C/ha), with a conservative estimate of 1,000 km² of hinterland area, the regional estimate of underground carbon in mangroves and associated halophyte scrubs rises to 96 Tg.

Discussion

Although mangroves have long been identified as important carbon sinks, few studies have focused on the mechanisms of belowground carbon storage. There is little information on how much carbon is stored below ground, in what form it is stored, and at what rates it accumulates. Perhaps the most important result of our study is that mangroves located in desert and dryland coasts can store comparable, and often higher, quantities of belowground carbon than their tropical counterparts, contributing disproportionately to the desert carbon pool.

Despite the short height (<3–4 m) and stunted appearance of these mangroves, the amount of belowground organic carbon stored in the topographically restricted mudflats of the Gulf of California was similar to the values we found in the lush mangrove forests of La Encrucijada, where the dominant *Rhizophora* trees are 30–40 m high, and also are within the range of values reported by Donato et al. (2) for tropical mangroves in the Indo-Pacific region.

Coastal Landscapes and Carbon Sequestration in Mangroves. The coastal landforms where the mangroves grow seem to play an important role in the amount of belowground storage. Although Balandra and Bahía Magdalena occur at similar latitudes and climates, the latter shows much lower values of belowground carbon storage. The main difference between the two ecosystems seems to be that Balandra has a pronounced relief where the extension of mangroves is largely constrained by the surrounding slopes, whereas Bahía Magdalena is part of a large, very flat coastal plain where a small increase in sea level will induce mangrove seedlings to establish inland (20). That is, as discussed by McKee (10), horizontally constrained mangroves tend to adjust to rising sea levels by rising gradually on their own peat, whereas mangroves in large, gently sloping coastal plains respond to changes in sea level or sedimentary accretion by establishing in new habitats, in effect moving the whole ecosystem horizontally as a result of environmental changes. Thus vertically accreting mangroves tend to accumulate large amounts of peat under their mudflats; horizontally dynamic mangroves in coastal plains tend to accumulate less organic matter in their substrate but often cover much larger areas because they tend to expand horizontally with sedimentary inputs (13). A test of this hypothesis is given by the Marismas Nacionales system, one of the best-studied cases of a Holocene shoreface succession. Its late-Holocene (<5,000 y B.P.) beach ridges are derived from the sediments from the three large rivers that feed the wetlands and make it one of the most dynamically accreting coasts in the world. The entire mangrove ecosystem has expanded into the ocean for the last 5,000 y, at a rate of 2 m/y in certain parts (21, 22, 23, 24), and, as a result, the carbon content in the sediments is the lowest of all our sampled cores.

Mangrove Peat. Different mangroves respond to rising sea levels according to the dominant landform where they grow. Peat in the Gulf of California region forms in mudflats under vertically accreting *Avicennia* mangroves growing in rocky bays and coves of

pronounced topography. Indeed, in all cases the exploration of topographically pronounced areas around the Bay of La Paz showed important layers of peat under the *Avicennia* mudflats. Healthy *Avicennia* mudflats accumulate 2–3 Mg C·ha⁻¹·y⁻¹. After three to five centuries, however, the remaining peat represents an accumulation rate of only ~0.4 Mg C·ha⁻¹·y⁻¹ (only 15–20% of the originally sequestered carbon). The rest, presumably, either has been washed away into the lagoon waters as soluble organic matter or has been re-emitted to the atmosphere as methane or carbon dioxide. Deep peat deposits may appear in the substrate of ecosystems that currently are not fixing large amounts of carbon, such as halophytic scrubs or receding shores with only dead stumps, showing that some coastal ecosystems may retain a large reservoir of carbon accumulated long ago.

Peat can accumulate in different ways depending on the dominant species in the forest. There was a marked difference between the peat formed under *Avicennia* mudflats in Balandra and that developed under *Rhizophora* mudflats in La Encrucijada. The root system of *Avicennia* trees radiates horizontally below ground, forming a layer of live roots some 30–40 cm below the surface of the mudflat. Above the root layer there is a layer of mangrove muck homogenized by the bioturbation that results from the activities of burrowing crabs and other detritivores. Thus, *Avicennia* trees develop roots immediately below the bioturbation muck layer; from this layer pneumatophores grow upwards to reach the surface, and roots grow down, forming the peat layer. In all cases, microscopy on peat cored below *Avicennia* mudflats confirmed that the peat remains were the result of belowground accumulation of refractory *Avicennia* roots (Fig. 3 A and B).

The mode of formation of *Rhizophora* peat in La Encrucijada is quite different. The roots of *R. mangle* branch off from stems, shoots, and secondarily thickened, anchored, aerial roots (Fig. 3 C and D). Lateral primary roots develop profusely from the stilt roots as soon as they hit the substrate. These lateral *Rhizophora* roots have little secondary thickening and form a dense, spongy reticulum that covers the mudflat surface. The trees basically stand on their stilt roots but have little deep anchoring and form peat [often used for palynological studies (25, 26)] on the surface of the mudflat (17).

Peat and Sea-Level Rise. The depth–age curve for the mangroves of Baja California indicates that sea level in the peninsula has been rising at a mean rate of 0.70 mm/y (SE \pm 0.07) during the last 17 centuries. This value does not differ significantly ($t = 0.71$, $P = 0.49$) from the value of 0.75 mm/y of sea-level rise rate for the last 2,000 y estimated by Toscano and McIntyre (7) for the Caribbean using *Acropora* corals and mangrove peat data. The presence of large amounts of mangrove peat in the rocky bays of the Gulf of California opens many possibilities for studying in detail the patterns of sea-level rise in the region.

The Role of Mangroves in the Regional Carbon Pool. Our results confirm the findings of Donato et al. (2), who characterized Asian mangroves as being extremely carbon-rich. Our carbon pool values and sequestration rates for La Encrucijada in Mexico were higher than those reported by Adame et al. (12), possibly because (i) we cored deeper for our total carbon estimations and (ii) we used mostly radiocarbon dating instead of the ash layer dating method, because the ash layer does not prevent some roots from tapping through and reaching below the dating layer. Zulueta et al. (15) showed that midday CO₂ sequestration fluxes in desert mangroves were almost one order of magnitude higher than in the surrounding desert scrub. Accordingly, warm deserts and tropical drylands have, on average, 14–20 Mg C/ha of belowground organic carbon, whereas the mudflat and fringe forests we studied in Baja California ranged between 463 and 1,130 Mg C/ha, 23–81 times larger than that of the surrounding desert scrub.

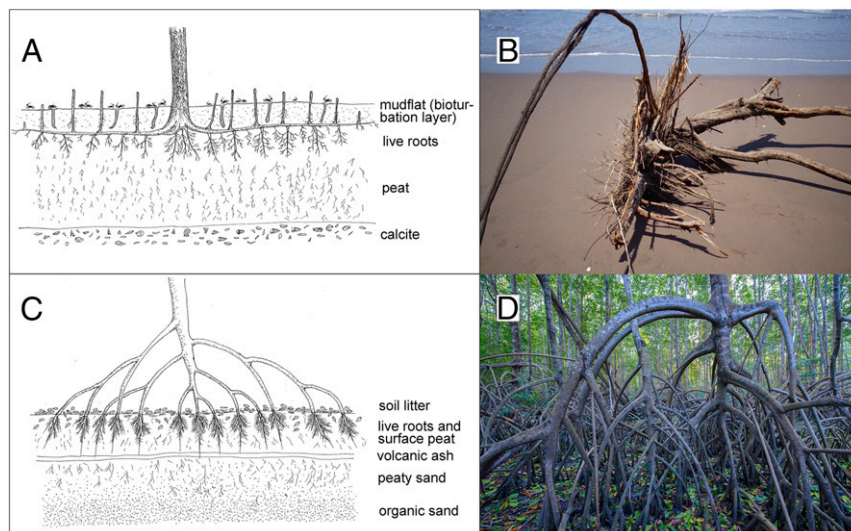


Fig. 3. Mangrove root systems and peat formation in mangroves. (A) The *Avicennia* root system at Balandra spreads underground, immediately below the clayey mudflat, forming a flat network of main roots from which pneumatophores emerge to the surface; fine roots are produced below the main root network, forming the underground peat deposits. (B) Individual of *A. germinans* eroded away by a hurricane at Marismas Nacionales, showing the horizontal network of main roots, the pneumatophores, and the peat-forming, downward-growing fine roots. (C) *As Rhizophora* root systems at La Encrucijada spread above ground, the individual roots produce abundant fine lateral roots after entering the substrate, forming dense peat deposits mixed with forest litter. (D) *Rhizophora* mudflat at La Encrucijada (illustration based on our own field observations and compared with descriptions from ref. 16).

Jointly, the 235,941 km² of drylands of Mexico's northwest store around 345 Tg of belowground carbon, whereas the coastal mangroves that fringe the coasts of these ecoregions, with an extent of only 1,162 km², store around 76 Tg of belowground carbon. With only 0.49% of the total area, the mangroves around the Gulf of California store 18% of the total belowground carbon pool of the whole region. If we add to this number the amount of carbon stored in sediments under halophyte scrubs (20 Tg), then mangroves and salty scrubs jointly store around 28% of the total belowground carbon pool in the region.

Methods

Study Sites. The two Baja California locations, Bahía Magdalena and Balandra, were sampled in September 2013. The tropical wetlands in the Pacific coast of mainland Mexico, Marismas Nacionales and La Encrucijada, were sampled in December 2014. Within each location, coring sites were chosen based on two criteria. In Baja California, sampling was systematically stratified into the three landforms that occur at varying distances from the water's edge: fringe, mudflat, and hinterland. We defined the area of forest that meets the lagoon water as the fringe. Moving inland, away from the water's edge, the mudflat, a flat, muddy expanse of forest, appears behind the fringe. Finally, the land-facing edge of the forest, where the mangroves become stunted in growth and begin to give way to other, usually small, halophilic plants, is called the "hinterland." Here the tide reaches very rarely, and the soil is drier and more saline because of the gently rising slope of the sedimentary plain. Mangrove zonation is more complex in tropical mainland Mexico than in Baja California, and sampling was focused around the dominant species present at each site, trying at all times to maintain the basic landform characterization of fringe–mudflat–hinterland. Detailed information on each site is provided in the *SI Text*.

Sampling Procedure. Using an open-faced soil sampler (Oakfield Apparatus), we cored into the substrate in 40-cm increments (the length of the corer). We described each distinct sediment layer along each core using the Geotechnical Gauge guide (W. F. McCollough) for color and texture definitions. Samples then were collected at every noticeable change in color or texture of the sediment layers. Extensions were used to continue coring and sampling until the corer could no longer penetrate the substrate, usually when densely compacted sand or a coarse calcite basement was reached. In addition to sampling the substrate, we collected live roots of nearby mangrove and deep belowground roots from the cores for tissue analysis and identification. We collected 17 samples from five sediment cores in Bahía Magdalena, 25

samples from six cores in Balandra, 12 samples from three cores in Marismas Nacionales, and 40 samples from five cores in La Encrucijada. All the sampling data and a detailed description of each core are provided in a publicly accessible data repository ([dx.doi.org/10.5061/dryad.5k0g4](https://doi.org/10.5061/dryad.5k0g4), also available at ezcurralab.ucr.edu/c-sequestration/mangroves.html).

Laboratory Analyses.

Carbon content. Each sample consisted of a core section 5 cm long, with a diameter of 1.7 cm, a cross-sectional area of 2.27 cm², and a cylindrical volume of 11.35 cm³. Samples were dried in an oven at 60 °C for 24 h and then were weighed on an analytical balance using aluminum weighing boats. The apparent density of the sample was obtained by dividing the mass of the core sample by the sample volume. After drying, samples were homogenized using an 8000D SPEX Dual Mill (SPEX SamplePrep). All samples were analyzed in a Carlo Erba NA1500 elemental combustion analyzer (Carlo Erba) to determine total carbon and nitrogen.

Multiplying the vertical extent of each layer by the apparent density, we obtained the mass per unit-area of each layer in the mangrove substrate; then, multiplying this mass by the percent organic carbon in that layer and summing these carbon masses for all layers in the sediment profile, we obtained the total mass of carbon per unit area at each site.

Peat and root microscopy. The collected live root and peat material was cut precisely under a dissection microscope to obtain thin tangential slices of root cortical tissue. The tissue then was stained using Trypan blue solution (0.4%) to color the cell wall structure selectively and identify morphological differences between *R. mangle* and *A. germinans*, the two dominant mangrove species in our sites.

Dating the sediments. Radiocarbon dating was performed at the Keck Carbon Cycle Accelerator Mass Spectrometry Facility in the Earth System Science Department at the University of California, Irvine. Results from the Keck laboratory were given as a fraction of the Modern Standard D¹⁴C and conventional radiocarbon age following Stuiver and Polach (27) and then were calibrated using one of two online programs: OxCal (<https://c14.arch.ox.ac.uk>) to calculate the probable age ranges for all samples preceding nuclear testing in 1950 and Calibomb (calib.qub.ac.uk/CALIBomb) for more recent, postbomb, samples. All dates were calculated in Gregorian, or calendar, years, and then were converted to years B.P. using 2015 (the year of the analysis) as the reference point.

In the two Baja California locations, we chose a subset of samples to undergo ¹⁴C radiocarbon dating to determine the age of the sediments. We dated different samples along the whole coring profile in three sites in Baja California: (i) a dead, receding, fringe in Bahía Magdalena, (ii) a hinterland with stunted *Avicennia* (but abundant belowground peat) in Balandra, and (iii) a peaty mudflat with dense stands of *Avicennia* in Balandra.

At La Encrucijada we took five peat subsamples in or near the first meter below the surface to estimate the rate of recent carbon accumulation in three different communities: a *Rhizophora*, a *Pachira*, and an *Avicennia* mudflat. Also at La Encrucijada, we took advantage of the layer of white, sandy clay found consistently below ground throughout the region, a product of the Santa Maria volcano eruption of October 1902. This eruption released a large cloud of volcanic ash that settled throughout the region and eventually was buried under new sediments (12). We used this layer to add a carbon accumulation rate estimate from an additional *Rhizophora* mudflat where we had not taken a radiocarbon sample. We did not use the volcanic ash layer as a dating reference in *Avicennia* or *Pachira* mudflats because root fragments immediately below the layer dated much younger than the layer itself, suggesting that younger roots were able to penetrate below the layer in their growth and hence the layer was not a reliable indicator of peat profile age.

Carbon Accumulation Rates. We first calculated the rate at which carbon has been sequestered in different ecosystems during recent times. For sites with ^{14}C dating, we took the core sample that was nearest to a century in age, calculated the total carbon in the sediment profile above that sample, and divided it by the age of the sample to obtain a mean carbon accumulation rate for the last century expressed in megagrams of carbon per hectare per year. In one site in La Encrucijada, where we did not perform radiocarbon dating, we used the layer of Santa Maria volcanic ash from the Chichonal eruption in October 1902 as a dating point. We calculated the total carbon in the sediment profile above the layer and divided it by 112.1 y, the time elapsed between the Chichonal volcanic explosion and our field sampling in 2014.

Combining the carbon–depth and the age–depth data, we created a carbon–age plot for the three sites in Baja California described above. To test how carbon accumulation scaled up with the age of the sediments, we fitted regression functions to different sections of the profile. Because both age and carbon measurements are subject to errors, we used major axis regression for this analysis.

Validating Results: Sampling Other Desert Mangroves. To validate our results from Balandra and Bahía Magdalena, in July 2014 M.T.C. sampled a series of small mangrove forests in the Gulf of California, near the Bay of La Paz. These sites included four topographically constrained inlets very similar in

landscape and topography to Balandra: El Merito (two cores), Puerto Gata (seven cores), San Gabriel (two cores), and San José (one core). In each site, we calculated the estimated belowground carbon content from each core.

Extrapolating Results: Geographic Information System Analysis. From Mexico's National Commission of Biodiversity (CONABIO) we obtained the latest map with the distribution of mangroves in Mexico including geospatial vector data (28) and calculated the area of mangrove forests found in the coasts of the drylands of northwestern Mexico, in the Baja California Peninsula, and the mainland states of Sonora and Sinaloa. Multiplying the area of mangroves by the mean amount of carbon stored under these mangroves, we obtained an estimate of the total amount of carbon stored below ground in the regional mangroves. We also downloaded the most recent vectorial data map of the terrestrial ecological regions of Mexico (29) available at CONABIO's website (www.conabio.gob.mx/informacion/gis/maps/geo/ecort08gw.zip) and calculated the area of the main dryland ecoregions around the Gulf of California, including (i) the Sonoran Desert, (ii) the Baja California Desert, (iii) the Sinaloa coastal thorn-scrubs, and (iv) the Cape Region thorn-scrubs. From the published literature (18) we then obtained an estimate of the amount of belowground carbon in each of these ecoregions and calculated an estimate of the total amount of belowground carbon stored in these drylands. We finally calculated the proportion of total carbon stored under mangrove forests in relation to other regional ecosystems.

ACKNOWLEDGMENTS. We thank J. Schimel at the University of California, Santa Barbara for advice and support throughout the study; C. González-Abraham for generously contributing the geographic information system analysis to this study; J. Cota-Nieto and K. Medeiros for assistance in sample collection; H. Yee, T. Abel, and the Isla Concepción project for help at La Encrucijada; J. Mata and the Ecomata staff for help at Marismas Nacionales; B. Deck for support in sample analysis; the Centro para la Biodiversidad Marina y la Conservación A.C. in La Paz for logistical support; K. LaFace and E. Navarro for assistance in sample processing; and the University of California Institute for Mexico and the United States for providing administrative and organizational support for our study. M.T.C. was supported by a National Science Foundation fellowship and by the Scripps Institution of Oceanography; part of this research was performed for his PhD dissertation. Funding was provided by the David and Lucile Packard Foundation, the Mia Tegner Memorial Fellowship, and the Helmsley Charitable Trust.

- Duarte CM, Cebrián J (1996) The fate of marine autotrophic production. *Limnol Oceanogr* 41(8):1758–1766.
- Donato DC, et al. (2011) Mangroves among the most carbon-rich forests in the tropics. *Nat Geosci* 4:293–297.
- Murdiyarmo D, et al. (2015) The potential of Indonesian mangrove forests for global climate change mitigation. *Nat Clim Chang* 5:1089–1092.
- McLeod E, et al. (2011) A blueprint for blue carbon: Toward an improved understanding of the role of vegetated coastal habitats in sequestering CO_2 . *Front Ecol Environ* 9(10):552–560.
- Siikamäki J, Sanchirico JN, Jardine SL (2012) Global economic potential for reducing carbon dioxide emissions from mangrove loss. *Proc Natl Acad Sci USA* 109(36):14369–14374.
- Murray BC (2012) Mangroves' hidden value. *Nat Clim Chang* 2(11):773–774.
- Toscano MA, Macintyre IG (2003) Corrected western Atlantic sea-level curve for the last 11,000 years based on calibrated ^{14}C dates from *Acropora palmata* framework and intertidal mangrove peat. *Coral Reefs* 22:257–270.
- Cahoon DR, et al. (2006) Coastal wetland vulnerability to relative sea-level rise: Wetland elevation trends and process controls. *Wetlands and Natural Resource Management*, eds Verhoeven JTA, et al. (Springer, Berlin), pp 271–292.
- McKee KL, Cahoon DR, Feller IC (2007) Caribbean mangroves adjust to rising sea level through biotic controls on change in soil elevation. *Glob Ecol Biogeogr* 16(5):545–556.
- McKee KL (2011) Biophysical controls on accretion and elevation change in Caribbean mangrove ecosystems. *Estuar Coast Shelf Sci* 91(4):475–483.
- McKee KL, Faulkner PL (2000) Mangrove peat analysis and reconstruction of vegetation history at the Pelican Cays, Belize. *Atoll Res Bull* 468:46–58.
- Adame MF, et al. (2015) Carbon stocks and soil sequestration rates of tropical riverine wetlands. *Biogeosciences* 12:3805–3818.
- Méndez-Linares AP, López-Portillo J, Hernández-Santana JR, Ortiz-Pérez MA, Oropeza-Orozco O (2007) The mangrove communities in the Arroyo Seco deltaic fan, Jalisco, Mexico, and their relation with the geomorphic and physical–geographic zonation. *Catena* 70(2):127–142.
- Anderson MS, Blake SF, Mehring AL (1951) *Peat and Muck in Agriculture*. Circular No. 888. (US Department of Agriculture, Washington, DC) 31 pp.
- Zulueta RC, et al. (2013) Aircraft regional-scale flux measurements over complex landscapes of mangroves, desert, and marine ecosystems of Magdalena Bay, Mexico. *J Atmos Ocean Technol* 30(7):1266–1293.
- Flores-Verdugo F, Day JWW, Briseño-Duenas R (1987) Structure, litterfall, decomposition, and detritus dynamics of mangroves in a Mexican coastal lagoon with an ephemeral inlet. *Mar Ecol Prog Ser* 35:83–90.
- Gill AM, Tomlinson PB (1977) Studies on the Growth of Red Mangrove (*Rhizophora mangle* L.) 4. The Adult Root System. *Biotropica* 9(3):145–155.
- Amundson R (2001) The carbon budget in soils. *Annu Rev Earth Planet Sci* 29:535–562.
- Búrquez A, Martínez-Yrizar A, Núñez S, Quintero T, Aparicio A (2010) Aboveground biomass in three Sonoran Desert communities: Variability within and among sites using replicated plot harvesting. *J Arid Environ* 74(10):1240–1247.
- López-Medellín X, Ezcurra E (2012) The productivity of mangroves in northwestern Mexico: A meta-analysis of current data. *J Coast Conserv* 16(3):399–403.
- Cisneros RA (2011) *Provenance and Origin of Holocene Beach Ridge and Modern Beach Sands from the Costa de Nayarit, Western Mexico*. M.S. thesis, Louisiana State University. Available at etd.lsu.edu/docs/available/etd-04262011-150353/. Accessed December 15, 2014.
- Curry JR, Emmel FJ, Crampton PJS (1969) Holocene history of a strand plain, lagoonal coast, Nayarit, Mexico. Coastal Lagoons, a Symposium, eds Ayala-Castañares A, Phleger FB (National Autonomous University of Mexico–United Nations Educational, Scientific, and Cultural Organization, Mexico City Mexico) pp. 63–100.
- Curry JR (1996) Origin of beach ridges. *Mar Geol* 136(1–2):121–125.
- Bhattacharya JP, Giosan L (2003) Wave-influenced deltas: Geomorphological implications for facies reconstruction. *Sedimentology* 50(1):187–210.
- Wooller MJ, Morgan R, Fowell S, Behling H, Fogel M (2007) A multiproxy peat record of Holocene mangrove palaeoecology from Twin Cays, Belize. *Holocene* 17(8):1129–1139.
- Joo-Chang JC, Islebe GA, Torrescano-Valle N (2015) Mangrove history during middle- and late-Holocene in Pacific south-eastern Mexico. *Holocene* 25(4):651–662.
- Stuiver M, Polach HA (1977) Reporting of ^{14}C data. *Radiocarbon* 19(3):355–363.
- CONABIO (2013) *Manglares de México: Extensión, Distribución y Monitoreo* (Comisión Nacional para el Conocimiento y Uso de la Biodiversidad – CONABIO, Federal District, México), 128 pp.
- Commission for Environmental Cooperation (2009) *Ecological Regions of North America: Toward a Common Perspective*. Online map (CEC, Montreal). Available at www.cec.org/tools-and-resources/map-files/terrestrial-ecoregions-level-ii. Accessed March 8, 2016.
- López-Medellín X, et al. (2011) Oceanographic anomalies and sea-level rise drive mangroves inland in the Pacific coast of Mexico. *J Veg Sci* 22(1):143–151.

Supporting Information

Ezcurra et al. 10.1073/pnas.1519774113

Detailed Information on Study Sites

Bahía Magdalena is a 200-km-long system of coastal lagoons separated from the ocean by a succession of sand bars and rocky islands. It harbors 226 km² of mangrove forests and represents the largest mangrove formation in the peninsula of Baja California (28). The lagoon complex is on the seaward edge of a large system of coastal plains that slope very gently into the Pacific Ocean, and for this reason it is particularly sensitive to changes in sea level (27). In the southern part of Bahía Magdalena, in a section called Bahía Almejas, we chose two sampling sites. The first one, Punta Cancún (N24°33' W111°44'), is an enclosed branch of the lagoon where mangroves apparently are in good health and the coast does not seem to be receding. The second site, La Salina (N24°34' W111°47'), corresponds to an exposed coastline that we knew from previous studies (30) has been receding as a result of sea-level rise and seawater thermal expansion during warm-phase anomalies in the Pacific Ocean.

Balandra is a small, 2-km-long lagoon system with an abrupt topography, harboring around 50 ha of mangrove forests. In contrast with the gently sloping plains of Bahía Magdalena, the mangrove coastline in Balandra is constrained by the surrounding mountains and cannot move appreciably inland with rising sea levels. The lagoon runs in a north-south direction with its mouth located roughly in the middle. We sampled two sites, one in the northern arm of the lagoon (N24°18' W110°19') and the second in the southern portion (N24°18' W110°18').

Marismas Nacionales (National Marshlands) is the largest (ca. 706 km²) tropical lagoon complex on the Pacific coast of North and South America (28). It lies in a flat coastal plain fed by three

sediment-rich rivers that descend from the Mexican highlands across the Sierra Madre: the Santiago, San Pedro, and Acajoneta Rivers. The most distinctive trait of this wetland is its strongly accretional nature and fast coastal dynamics: A series of beach ridges that started to grow some 5,000 y ago now separates the mid-Holocene coastal lagoons from the ocean by a parallel succession of beach ridges that is, in parts, more than 10 km wide (22–24). We sampled two sites near the coast of the San Pedro/Toro Mocho river systems. The first site, Camichín (N21°45' W105°28'), harbored a forest of black mangrove (*A. germinans*) and was near the confluence of the two rivers. The second, upstream, site, Arroyo Toro Mocho (N21°46' W105°28'), harbored a low, sparse *Avicennia* forest.

La Encrucijada is a 40-km-long system of coastal wetlands and tropical lagoons on the Pacific Coast of Chiapas near the Guatemalan border. Fed by a series of relatively small rivers that descend from the mountains of El Soconusco, it sustains 294 km² of mangrove forests (28), including some of the tallest mangroves in Mexico, with trees reaching 40 m in height. The dominant species in the basin floodable mudflats is the red mangrove, *R. mangle*, in sharp contrast with other mangroves in Mexico where mudflats normally are colonized by *A. germinans* trees. We sampled three locations: La Concepción (N15°03' W092°44'), a floodable island covered by tall *Rhizophora* forest; Aztlán (N15°01' W092°40'), a riparian coastal plain covered by the freshwater swamp tree *P. aquatica*; and Las Garzas (N15°12' W092°48'), an inland saline mudflat covered by a monospecific *Avicennia* forest, which is otherwise rare in this region.

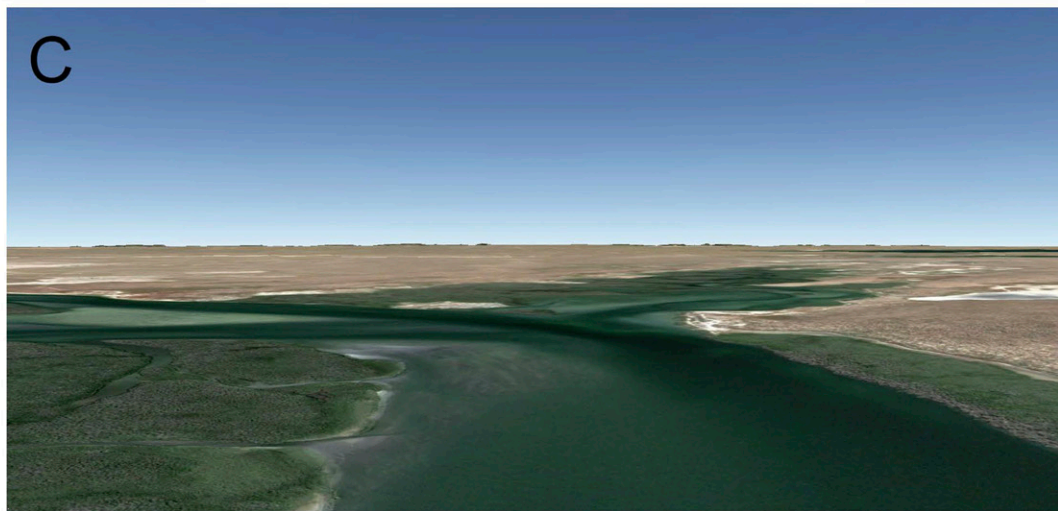
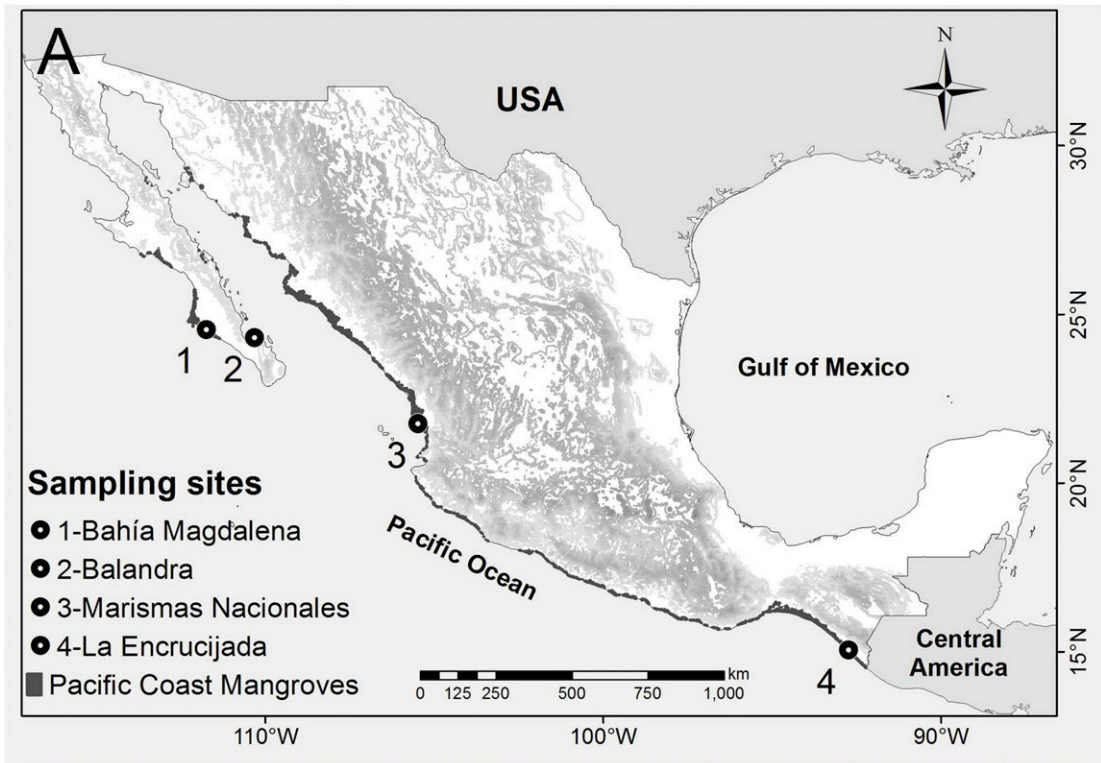


Fig. S1. Sampling sites' location and relief. (A) Map of Mexico with the four sampling sites. Image courtesy of INEGI online shapefiles, www.inegi.org.mx. (B) Projected satellite image of Balandra, an enclosed, topographically constrained inlet bordered with mangrove forests. (C) Projected satellite image of Bahía Magdalena, a flat coastal plain where the establishment of new mangroves can move inland easily with small increases in sea level. In both images there is no vertical exaggeration (vertical-to-horizontal scale 1:1). Map data: Google, DigitalGlobe.

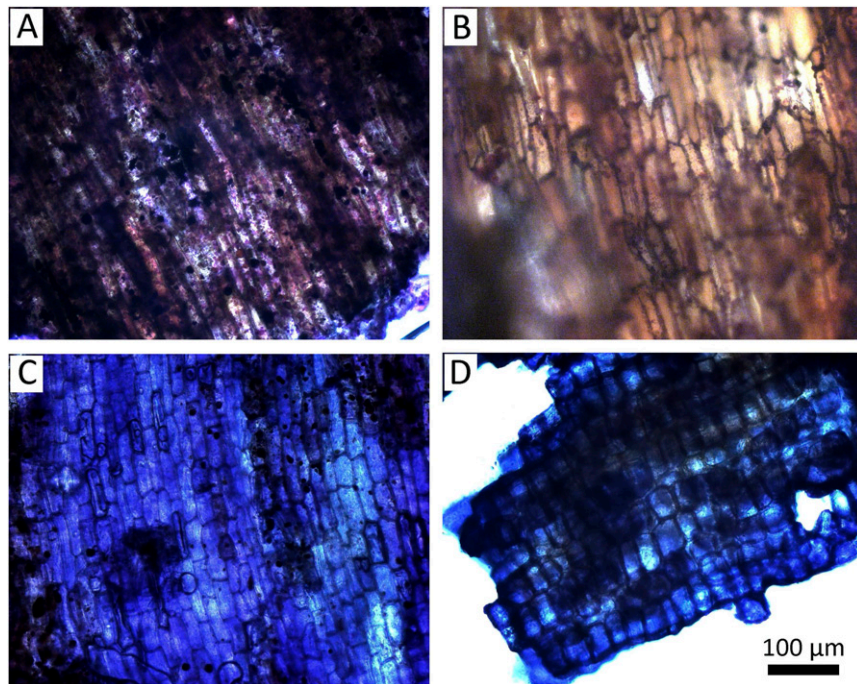


Fig. S2. Microscopic image of the epidermal tissue cells separated from peat samples and living roots. Balandra peat (A) and Bahía Magdalena peat (B) samples, both taken at ca. 1 m deep. When these images are compared with images of the epidermis from live roots of *A. germinans* (C) and *R. mangle* (D), it is clear that the peat is derived from *Avicennia* roots. (C) Note the longitudinally elongated rows of the *Avicennia* cells, each 50–70 μm long and 10–20 μm wide, similar in size and shape to those in the peat samples. (D) The cells in *Rhizophora* are shorter (20–30 μm long) and wider (30–40 μm wide).

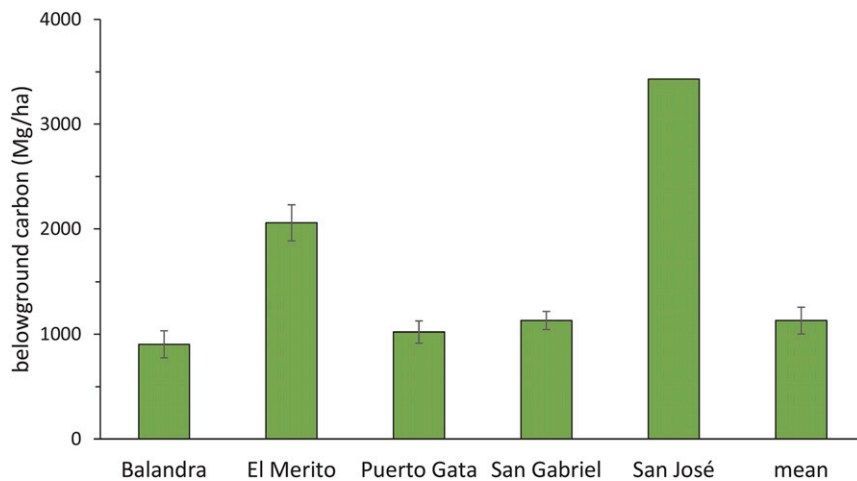


Fig. S3. Total belowground carbon stored in peaty, vertically accreting mudflats in the Gulf of California. The bar on the right shows the overall mean for all cores sampled in the region.

Dataset S1. Summary tables of core data

[Dataset S1](#)

A complete repository of all of the sampling data and a detailed description of each core are provided in a publicly accessible data repository (dx.doi.org/10.5061/dryad.5k0g4, or, alternatively, ezcurralab.ucr.edu/c-sequestration/mangroves.html). The main data are presented in this dataset.

Bahía Magdalena

depth (cm)	sample depth (cm)	color	texture	δ (g/cm ³)	% C	C (Mg/ha)	total C (Mg/ha)
Core 1: Punta Cancún, <i>Rhizophora</i> fringe (N24°33'04.1" W111°44'14.2")							
0–10	3-7	olive-brown gray	loamy sand	0.71	2.33	16.64	503.0
10–25	20-25	reddish-olive gray	loamy peat	0.74	6.07	67.34	
25–40	35-40	reddish-olive gray	loamy peat	0.85	7.44	94.77	
40–100	95-100	greenish-olive gray	sandy	1.83	2.77	303.87	
100–125	120-125	greenish-olive gray	sandy	2.95	0.28	20.45	
Core 2: Punta Cancún, <i>Avicennia</i> upper mudflat/hinterland (N24°33'02.1" W111°44'13.6")							
0–12	5-10	olive-gray	peaty-loamy sand	1.26	1.26	19.09	93.1
12–80	40-45	olive gray	loamy sand	2.15	0.51	73.98	
Core 3: La Salina, receding, dead mangrove fringe (N24°34'35.6" W111°48'02.2")							
0–5	4-9	orange-brown	sandy	1.07	2.47	13.23	440.6
5–45	41-46	orange-brown	sandy, then sandy peat	0.74	1.17	34.85	
45–76	116-121	reddish olive gray	sandy peat	1.84	6.41	364.66	
76–125	142-147	dark-olive gray peat, then light-gray sand	peat, to sandy-organic	2.21	0.26	27.87	
Core 4: La Salina, <i>Rhizophora</i> fringe (N24°34'35.3" W111°48'02.0")							
0–9	0-5	reddish-brown	peaty	1.67	0.72	10.88	446.0
9–46	40-45	reddish-brown	peaty	2.04	1.42	107.21	
46–121	71-76	olive gray	peaty sand	1.22	3.39	310.44	
121–147	105-110	dark-olive gray	sandy-organic	1.89	0.35	17.43	
Core 5: La Salina, <i>Avicennia</i> upper mudflat/hinterland (N24°34'38.2" W111°47'56.3")							
0–9	4-9	olive-gray, to light olive gray	sandy peat	1.38	1.95	24.22	161.7
9–120	38-43	light gray	sandy peat to organic sand	2.55	0.49	137.45	

Balandra

depth (cm)	sample depth (cm)	Color	texture	δ (g/cm ³)	% C	C (Mg/ha)	total C (Mg/ha)
Core 1: Sur, <i>Avicennia</i> mudflat (N24°18'38.3" W110°19'05.9")							
0–40	0-5	reddish olive-gray	sandy clay	1.47	0.70	41.14	477.6
40–120	47-52	reddish olive-gray	peaty sandy clay	1.76	0.82	115.07	
120–173	167-173	reddish peat	peat (spongy)	0.79	6.42	270.01	
173–200	180–185	reddish peat	peat (spongy)	1.58	1.20	51.41	

depth (cm)	sample depth (cm)	Color	texture	δ (g/cm ³)	% C	C (Mg/ha)	total C (Mg/ha)
Core 2: Sur, <i>Avicennia</i> upper mudflat/hinterland (N24°18'36.8" W110°19'06.8")							
0–8	0-5	olive-brown	loamy clay	1.22	1.11	10.86	1191.8
8–45	40-45	olive-brown	loamy clay	1.94	0.37	26.42	
45–118	113–118	45-110: olive-greenish gray; at 110 cm brown-reddish peat	45-110: loamy clay; at 110 cm brown-reddish peat	1.25	3.74	341.44	
118–160	155-160	brown-reddish peat	peaty	1.39	4.39	391.80	
160–182	177-182	olive gray	peaty sand	1.42	2.83	257.68	
182–220	190-195	olive-blue gray	peaty sand	0.97	2.65	97.58	
220–226	221-226	white calcite	sandy gravel	1.95	5.66	66.03	
Core 3: Sur, <i>Rhizophora</i> fringe (N24°18'44.3" W110°19'00.8")							
0–45	7-12	dark-gray	sandy calcite with organic mud	1.70	0.44	33.82	279.4
45–163	155-160	dark-gray	sandy calcite with organic mud	3.26	0.52	198.12	
163–200	184-188	light-gray with whitish calcite grains	sandy calcite with organic mud	1.88	0.68	47.43	
Core 4: Norte, <i>Rhizophora</i> fringe (N24°19'19.4" W110°19'00.5")							
0–9	4-9	olive gray	calcite fragments in surface, then peaty loam	0.74	9.61	63.68	893.8
9–43	38-43	9-40: dark peat 40-43: whitish	muddy peat and calcite coarse sand	1.11	11.15	418.90	
43–61	56-61	whitish	calcite coarse sand	2.17	10.51	411.18	
Core 5: Norte, <i>Avicennia</i> mudflat (N24°18'53.7" W110°18'53.2")							
0–9	0-5	olive-gray	loamy clay	0.64	3.53	20.27	1289.1
9–45	40-45	reddish peat in olive-gray mud	clayey peat	0.49	17.34	303.30	
45–119	114-119	reddish peat in olive-gray mud	peat	0.56	13.92	581.32	
119–145	140-145	red peat on a red-olive matrix	peat with fragments of calcite	0.45	11.62	134.96	
145–184	179-184	red peat, last 15 cm whitish fragments of calcite	peat with fragments of calcite	1.33	4.79	249.25	
Core 6: Norte, <i>Avicennia</i> upper mudflat/hinterland (N24°18'53.8" W110°18'52.7")							
0–49	4-9	light gray	loamy clay	1.44	0.60	42.27	966.5
49–197	121-126	reddish peat with olive-gray mud matrix	peaty with a clayey matrix	0.75	7.29	812.45	

depth (cm)	sample depth (cm)	Color	texture	δ (g/cm ³)	% C	C (Mg/ha)	total C (Mg/ha)
197–210	201–206	reddish with white grains	peaty calcite sand	1.06	8.09	111.83	

Marismas Nacionales

depth (cm)	sample depth (cm)	color	texture	δ (g/cm ³)	% C	C (Mg/ha)	total C (Mg/ha)
------------	-------------------	-------	---------	-------------------------------	-----	-----------	-----------------

Core 1: Camichín, *Avicennia* upper mudflat/hinterland (N21°45'39.4" W105°28'41.8")

0–40	30–35	grayish with olive-blue pockets, & spots of reddish peat	clayey with live roots	1.50	1.18	70.74	167.7
40–80	70–75	same	Clayey	1.15	1.19	54.52	
80–120	110–115	same	sandy	1.24	0.78	38.61	
120–130	120–125	same	sandy, strongly compacted	1.64	0.23	3.79	

Core 2: Camichín, *Avicennia* mudflat (N21°45'41.3" W105°28'40.5")

0–40	30–35	grayish with olive-blue pockets, & spots of reddish peat	loamy with live roots	1.41	1.02	57.68	132.7
40–80	70–75	same	loamy	1.74	0.55	38.14	
80–115	105–110	same	sandy, strongly compacted	1.63	0.65	36.85	

Core 3: Arroyo Toro Mocho, *Avicennia* mudflat/hinterland (N21°46'6.70" W105°28'2.80")

0–40	35	grayish with olive-blue pockets, & spots of reddish peat	loamy with live roots	1.62	2.29	148.17	225.7
40–54	49–54	same	loamy	1.51	0.39	8.17	
54–80	79–75	same	loamy	1.50	0.61	23.61	
80–120	110–115	Same	sandy	2.02	0.42	34.09	
120–160	150–155	Same	sandy, strongly compacted	2.02	0.14	11.64	

La Encrucijada

depth (cm)	sample depth (cm)	color	texture	δ (g/cm ³)	% C	C (Mg/ha)	total C (Mg/ha)
------------	-------------------	-------	---------	-------------------------------	-----	-----------	-----------------

Core 1: La Concepción, *Rhizophora* mudflat (N15°03'54.5" W092°45'03.2")

0–10	0–5	brownish	leaf litter	0.25	37.00	92.28	2025.4
10–55	40–45	reddish	peat	0.39	32.44	575.34	

depth (cm)	sample depth (cm)	color	texture	δ (g/cm ³)	% C	C (Mg/ha)	total C (Mg/ha)
55–75	65–70	whitish-gray	white sandy clay	0.95	1.68	31.89	
75–90	75	dark brown	organic matter	0.39	18.35	107.66	
90–105	95–100	dark brown	clayey peat	0.83	10.60	131.74	
105–140	115–120	dark brown	clayey peat	0.90	7.84	246.34	
140–180	155–160	dark brown	clayey peat	1.08	6.27	270.23	
180–215	195–200	dark brown	peaty loamy sand	0.75	7.76	203.89	
215–235	230–235	dark brown	peaty loamy sand	0.68	11.38	155.08	
235–255	235–240	dark brown	loamy sand	1.55	4.27	132.48	
255–290	275–280	dark brown	loamy sand	1.79	1.06	66.28	
290–300	295–300	dark brown	highly compacted organic sand	2.15	0.57	12.20	
Core 2: La Concepción, <i>Rhizophora fringe</i> (N15°04'08.5" W092°45'28.2")							
0–10	0–5	Reddish	peat	0.60	7.66	46.20	615.0
10–55	35–40	dark brown	water-logged loamy mud	1.47	1.07	70.92	
55–105	76–81	greenish-gray	water-logged sand	0.79	2.50	98.65	
105–135	115–120	olive-gray	organic loamy sand	2.11	1.07	67.41	
135–170	155–160	dark gray	organic sand	1.80	4.72	298.13	
170–185	180–185	dark gray	organic sand	2.21	1.02	33.66	
Core 3: Aztlán, <i>Pachira aquatica</i> mudflat (N15°01'16.9" W092°40'32.6")							
0–5	0–5	dark reddish	peat-like	0.25	37.94	46.61	1466.2
5–20	5–10	grayish-white	white sandy-clay	0.52	25.72	200.33	
20–70	35–40	grayish	organic loam	0.22	5.31	59.73	
70–135	100–105	grayish	clay	1.07	3.93	273.33	
135–185	170–176	olive-gray, with lumps of red peat	compacted clay with lumps of peat	0.55	8.11	222.46	
185–220	195–200	dark olive-gray	organic sandy loam	1.80	1.46	91.90	
220–255	235–240	dark brown	root-rich sandy loam	0.88	6.47	199.16	
255–305	270–275	dark brown	fine clayey sand	1.70	2.76	234.72	
305–350	345–350	dark brown	fine clayey sand	1.21	2.53	137.96	
Core 4: Las Garzas, <i>Avicennia</i> mudflat (N15°12'14.6" W092°48'46.7")							
0–20	0–5	brownish	leaf litter	0.54	6.12	66.47	462.5
20–105	35–40	olive-gray	clay	1.39	0.79	54.60	
105–185	110–115	olive-green	clay	1.40	0.25	27.67	
185–205	190–195	olive to grayish-white	clay	1.29	0.40	10.25	
205–230	215–220	dark brown	organic loam	0.92	7.51	172.91	
230–240	235–240	dark brown mixed with gray	organic loam mixed with clay	1.48	1.95	28.88	
240–255	240–245	reddish	clayey peat	0.62	10.57	97.63	
255–265	260–265	dark olive-gray	clay with fine sand	1.55	0.26	4.05	

depth (cm)	sample depth (cm)	color	texture	δ (g/cm ³)	% C	C (Mg/ha)	total C (Mg/ha)
Core 5: La Concepción, <i>Rhizophora</i> mudflat (N15°03'34.1" W092°44'42.4")							
0–35	0–5	dark reddish brown	root and detritus	0.18	41.32	252.39	831.1
35–45	40–45	whitish-gray	white sandy clay	1.43	2.44	34.99	
45–95	75–80	dark brown	organic loam	1.37	4.66	320.02	
95–135	110–115	dark brown	organic loamy sand	1.57	2.24	140.90	
135–155	145–150	dark brown	organic sand	1.48	2.80	82.78	